ACS APPLIED MATERIALS & INTERFACES

www.acsami.org

Research Article

Photoelectrochemical Sensing of α-Synuclein Based on a AuNPs/Graphdiyne-Modified Electrode Coupled with a Nanoprobe

Ting Yao, Ruhao Wang, Yuchan Meng, and Xu Hun*

Cite This: *ACS Appl. Mater. Interfaces* 2021, 13, 26515−26521

Read Online

ACCESS | Metrics & More | Article Recommendations | Supporting Information

ABSTRACT: We developed a method for photoelectrochemical (PEC) sensing based on a AuNPs/graphdiyne, as a low background signal composite material, modified electrode coupled with a nanoprobe (probe DNA/DA/MBA/WSe_2) for sensitive α-synuclein (α-Syn) detection. A tungsten selenide (WSe_2) nanoflower was first produced with a one-pot solvothermal method and employed as a signal amplification element and the modified substrate of the nanoprobe. The synergy effect between the WSe_2 nanoflower and graphdiyne (GDY) can reduce the photoinduced electron−hole recombination and expedite the spatial charge separation. Due to the synergistic effect of AuNPs/GDY and WSe_2, this detection strategy provides a high signal-to-noise ratio and good performance. The signal indicator, dopamine/4-mercaptophenyl boronic acid/WSe_2 (DA/MBA/WSe_2), was generated with the recognition of boron−diol. In the presence of the α-Syn oligomer, the target triggered cycle I strand displacement amplification and achieved the conversion of the α-Syn oligomer to a massive output of false-target DNA (FT). The output FT was used for the cycle II catalytic hairpin assembly onto the electrode which was modified with AuNPs/GDY and triple-stranded DNA (TsDNA); thereby, plenty of PEC nanoprobes which are composed of probe DNA and the signal indicator are captured, and the photocurrent response is produced correspondingly. This PEC biosensor generated a strong photocurrent with low blank (27.6 nA) and was sensitive to α-Syn oligomer. The limit of detection was 3.3 aM, and the relative standard deviation (RSD) was 3.7% at 100 aM. Moreover, it also has good selectivity, indicating promising potential in clinical diagnostics.

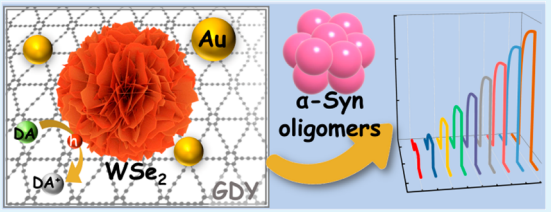

KEYWORDS: *photoelectrochemistry, graphdiyne, WSe_2 nanoflower, nanoprobe, α-synuclein*

INTRODUCTION

The specific and sensitive determination of nucleic acids or protein biomarkers offers one of the most attractive solutions to deal with clinical diagnosis, mutation detection, and cancer therapy.[1−3] The photoelectrochemical (PEC) method is a promising means because it has a lot of advantages such as rapid response and high sensitivity.[4,5] As we all know, appropriate photoactive materials are a crucial parameter for photoelectric conversion efficiency which affects the PEC-sensitive assay. As an excellent photoelectric material, WSe_2 has been utilized in PEC biosensors owing to its good optoelectronic properties.[6,7] However, the band gap of WSe_2 is ∼1.5 eV,[8] which often leads to the disadvantage of insufficient utilization of light energy owing to the relatively wide band gap.[9] Indeed, some metal-free carbonaceous materials exhibit significant positive effects on separating photoinduced electron−hole pairs and improving the photocatalytic performance of other semiconductor materials.[10,11] Graphdiyne (GDY) is a promising substrate for immobilizing metal particles and nanomaterials, which makes it useful as a high-performance biosensor. GDY is a new carbonaceous material composed of atom networks with sp- and sp^2-hybridized carbon. The unique benzene ring structure endows GDY with a higher π-conjugated structure than graphene, which is favorable for electronic transmission and conductivity.[10] Furthermore, unlike graphene with zero band gap, which requires additional doping, GDY is a self-doped material and naturally has charge carriers.[12,13] So, this low band gap material can be used to suppress electron−hole recombination and is advantageous to the light absorption range. Gold nanoparticles (AuNPs) show better conductivity. Owing to these attributes, the introduction of GDY and AuNPs is expected to improve the photocatalytic performance of WSe_2.

In addition, it is important to get high sensitivity to improve the accuracy of a biosensor. To achieve this goal, one of the means is to produce a large PEC signal; another method is to reduce the background signal and improve the signal-to-noise ratio (S/N). In traditional biosensors, the material is directly modified on the electrode, which is inevitable to obtain a high PEC signal. However, it will also result in a high background signal and reduce the S/N and sensitivity. On the other hand,

Received: April 26, 2021
Accepted: May 18, 2021
Published: June 1, 2021

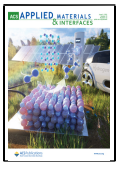

https://doi.org/10.1021/acsami.1c07617
ACS Appl. Mater. Interfaces 2021, 13, 26515−26521

the system will produce a strong PEC response under illumination when the photoelectric material encounters the electron donor or acceptor. In order to obtain the signal with low background and high response in the presence of a target, it is an effective strategy to use a photoelectric material with a small background signal as the substrate and a photoelectric material with a higher signal as the probe. This strategy will lead the PEC biosensor to present an intense photocurrent signal only when the target exists.

α-Synuclein (α-Syn) oligomer is commonly associated with Parkinson's disease and dementia with Lewy bodies.[14−16] Thus, α-Syn oligomer is used as an important target for the diagnosis of cerebrospinal fluid and plasma of Parkinson's disease patients.[15,17] So far, the methods that have been developed to detect α-Syn include fluorescence,[18] NMR spectroscopy,[19] surface plasmon resonance (SPR),[20,21] colorimetry,[20] and so forth. But these methods need complex instruments and are time-consuming, with insensitive detection. The strategy of combining an aptamer and PEC analysis is adopted to detect α-Syn that can report a signal with an ultrahigh sensitivity and a wide response range. In this work, an ultrasensitive PEC biosensor was constructed based on AuNPs/GDY as the substrate, WSe_2 nanoflower as the signal enhancer, and a combined dual-signal amplification strategy for determination of α-Syn oligomer. The WSe_2 nanoflower was successfully prepared via a one-pot solvothermal method. The signal indicator, dopamine/4-mercaptophenyl boronic acid/WSe_2 (DA/MBA/WSe_2), was generated by a stepwise chemical reaction strategy. When the thiol-modified probe DNA was labeled onto the signal indicator, DA/MBA/WSe_2, the PEC nanoprobe, DA/MBA/WSe_2/PD, was obtained. The PEC nanoprobe hybridized with the capture DNA which was immobilized onto AuNPs/GDY/GE (AuNPs/GDY nanocomposite modified gold electrode) in the presence of α-Syn oligomer. The strong PEC signal was produced with the help of the dual-signal amplification strategy. Without the α-Syn oligomer, no PEC nanoprobe was captured, which means that the PEC signal was only produced from AuNPs/GDY, and a low background signal is obtained. On the basis of this, an ultralow background signal and high sensitivity are gained.

EXPERIMENTAL SECTION

Synthesis of AuNPs/GDY. The substrate material GDY was donated by Professor Yuliang Li (Institute of Chemistry, Chinese Academy of Sciences, Beijing, China). As reported previously, the GDY is synthesized with a cross-coupling reaction (Supporting Information S3).[22,23] Then, GDY was exfoliated and dispersed in dimethylformamide (DMF) to prepare a 2 mg/mL dispersion liquid (Supporting Information S4). To prepare AuNPs/GDY, 4.95 mL of GDY solution was sonicated for 30 min. Then, 50 μL of 1 wt % $HAuCl_4$ solution and 100 μL of 10 wt % sodium citrate solution were added under stirring for 1 h at 80 °C. Eventually, the obtained product, AuNPs/GDY, was centrifuged at 10 000 rpm, and then washed by ultrapure water three times. Then, it was redispersed in DMF and stored at 4 °C.

Synthesis of the WSe_2 Nanoflower. Amounts of 0.64 g of selenium and 0.20 g of $NaBH_4$ were mixed in 60 mL of DMF. Then, the mixture was continuously stirred until the solution turned red. Afterward, 0.98 g of $(NH_4)_6H_2W_{12}O_{40}\cdot nH_2O$ was added. The mixed solution was transferred and sealed in a Teflon-lined stainless-steel autoclave at 240 °C for 12 h. After cooling down to room temperature naturally, the resulting precipitate was centrifuged at 10 000 rpm, purified with deionized water and ethanol three times, and finally dried under vacuum for 12 h to obtain the WSe_2 nanoflower.

Synthesis of the Signal Indicator. A stepwise chemical reaction strategy based on the sulfur−metal bond[7,24] and the specific recognition of boronic acid to diols[25−27] was designed to manufacture the signal indicator for signal amplification. First, 1 mL of 2 mg/mL WSe_2 nanoflower was premixed with 0.75 mg of 4-mercaptophenyl boronic acid (MBA), and then allowed to incubate for 18 h at the room temperature at 110 rpm. Subsequently, dopamine (DA) with the same concentration as MBA was added, and the mixture was incubated in the dark for 3 h. Finally, unattached substances were removed by centrifugal washing to obtain the DA/MBA/WSe_2 signal indicator.

Preparation of the PEC Nanoprobe. An amount of 100 μL of 10 μM probe DNA (PD) solution was mixture with 400 μL of DA/MBA/WSe_2 and stirred overnight (Scheme 1A) to get the PEC nanoprobe, DA/MBA/WSe_2/PD.

Scheme 1. Schematic Illustration of the PEC Strategy for α-Syn Detection[a]

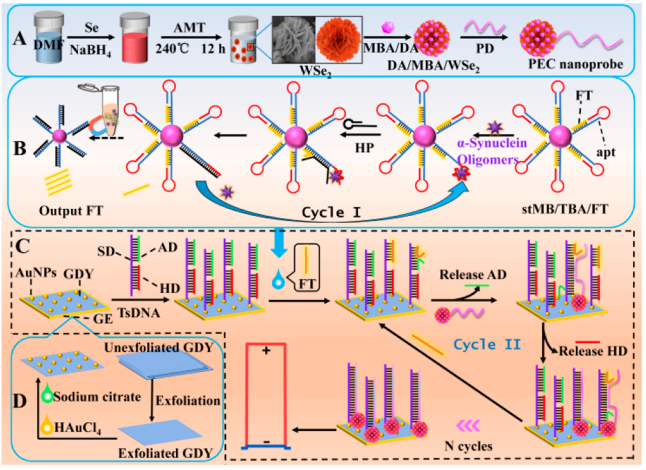

[a]Preparation of the WSe_2 nanoflower with a one-pot solvothermal method and DA/MBA/WSe_2 with the MBA-linking strategy (A); principle of the α-Syn-triggered cycle I (B); cycle II triggered by output FT onto the surface of the modified electrode and PEC response in the absence of target (−) and in the presence of target (+) (C); preparation of AuNPs/GDY/GE (D).

Detection of the α-Synuclein Oligomer. First, 20 μL of 2 μM aptamer (apt) was mixed with 20 μL of 2 μM false-target DNA (FT) at 37 °C for 2 h to form dsDNA. Then, the mixture was added into 40 μL of streptavidin-modified magnetic beads (stMB) and incubated for 0.5 h at 37 °C under stirring, thus obtaining the stMB/apt/FT complex through biotin−streptavidin bonding. Subsequently, 20 μL of α-Syn oligomer and 1 μM hairpin DNA (HP) were added and incubated 2 h at 37 °C. In the meantime, the gold electrode (GE) was modified with 15 μL of 2.5 mg/mL AuNPs/GDY and triple-stranded DNA (TsDNA) (Supporting Information S5). After magnetic separation, the separation solution was dropped onto the modified electrode. Then, 20 μL of PEC nanoprobe was dropped. After incubation at room temperature for 2 h the electrode was rinsed with phosphate buffer and the PEC measurement was executed (Supporting Information S6).

RESULTS AND DISCUSSION

Principle of PEC Sensing. As exhibited in Scheme 1, the WSe_2 nanoflower was prepared with a solvothermal method. Then, DA/MBA/WSe_2 and the PEC nanoprobe are synthesized (Scheme 1A). stMB/apt/FT consisted of streptavidin-modified magnetic beads, aptamer, and FT DNA. In the presence of α-Syn oligomer, the target triggered cycle I and achieved the conversion of α-Syn oligomer to a

https://doi.org/10.1021/acsami.1c07617
ACS Appl. Mater. Interfaces 2021, 13, 26515−26521

massive output of FT (Scheme 1B). The output FT was used for cycle II onto the surface of electrode which was modified with AuNPs/GDY and TsDNA (Scheme 1, parts C and D).[28] Ulteriorly, plenty of PEC nanoprobes are captured, and the photocurrent response is produced correspondingly (Supporting Information S13).

Characterization of the Nanomaterials. After exfoliating, the thickness of the GDY became significantly thinner than that of unexfoliated GDY (Figure S1). As seen in Figure 1,

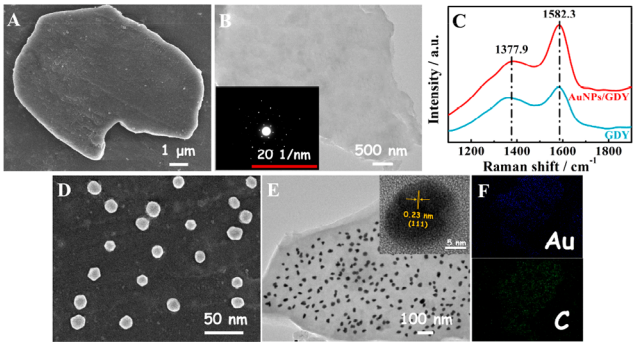

Figure 1. SEM (A) and TEM (B) images of exfoliated GDY. Raman spectra of GDY (C). SEM (D), TEM (E), and elemental mapping (F) images of AuNPs/GDY. The inset in panel B is the SAED of GDY. The inset in panel E is the HRTEM of the AuNPs.

parts A and B, exfoliated GDY displayed a very smooth surface and thin-layered structure. The hexagonal pattern two-dimensional (2D) periodicity revealed by the selected area electron diffraction (SAED) showed that exfoliated GDY had high crystallinity (the inset in Figure 1B). For the AuNPs/GDY (Figure 1, parts D and E), it was clear that AuNPs with an average diameter of ca. 16 nm are homogeneously distributed onto the surface of GDY. Furthermore, the uniform distribution of C and Au on the AuNPs/GDY was shown by energy dispersive spectrometry (EDS) (Figure 1F). After depositing AuNPs, the Raman characteristic peaks of GDY are significantly enhanced (Figure 1C). These results indicated the successful deposition of AuNPs on the GDY.

Scanning electron microscopy (SEM) images show that WSe_2 possesses a flower-like structure, the WSe_2 nanoflower is assembled by folding a thin layer, and the diameter of the WSe_2 nanoflower is about 150 nm (Figure 2A). In the high-

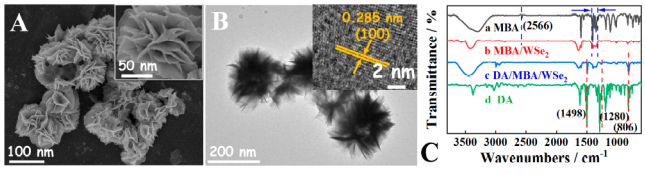

Figure 2. SEM (A) and TEM (B) images of the WSe_2 nanoflower. (C) FT-IR spectra of MBA (a), MBA/WSe_2 (b), DA/MBA/WSe_2 (c), and DA (d). The magnification (inset in panel A) and HRTEM (inset in panel B) of the WSe_2 nanoflower.

resolution transmission electron microscopy (HRTEM) images, it can be seen that clear lattice fringes appear (Figure 2B). The lattice spacing is 0. 285 nm, which is in good agreement with the lattice spacing of the (100) crystal plane in the standard X-ray diffraction (XRD) pattern of WSe_2.[29,30] MBA/WSe_2 and DA/MBA/WSe_2 were also characterized (Figure S2). After modification with DA and DA/MBA, the nanoflowers remained in a good dispersion.

Photoelectric Properties of the Nanomaterials. The PEC properties of photoactive materials, including GDY, AuNPs/GDY, and WSe_2–AuNPs/GDY, were measured (Figure 3 and Figure S3). WSe_2–AuNPs/GDY was obtained

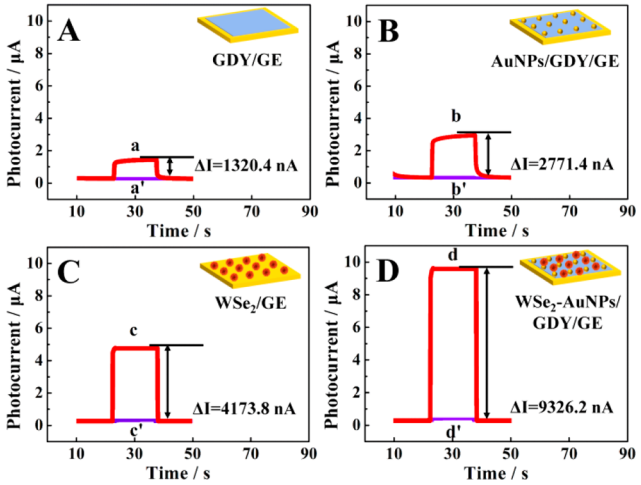

Figure 3. PEC responses of different nanomaterials: GDY (A), AuNPs/GDY (B), WSe_2 (C), and WSe_2–AuNPs/GDY (D) in phosphate buffer containing or not containing DA (10 μM).

by dropping 15 μL of WSe_2 nanoflower suspension onto the surface of a AuNPs/GDY-modified electrode, and it is utilized to confirm that WSe_2 can immensely help AuNPs/GDY enhance the PEC signal. Herein, DA is used as the electron donor for the PEC signal amplification. The PEC signal of exfoliated GDY is 3 times higher than that of the primary untreated GDY in the presence of DA (Figure S4). It suggested that the exfoliated GDY has a more excellent photoelectric response, and all subsequent GDY represents the exfoliated GDY. The PEC signal of GDY in the absence and presence of DA is 12.6 nA (Figure 3A, curve a′) and 1333.0 nA (Figure 3A, curve a), respectively. For the AuNPs/GDY, the photocurrent response (Figure 3B, curve b′, 27.6 nA; Figure 3B, curve b, 2799.0 nA) was about 2-fold higher than that of GDY, which was attributed to the excellent conductivity of AuNPs, and the PEC responses of the AuNPs were 9.7 and 32.5 nA (Supporting Information S12). In addition, the PEC responses of WSe_2 are 150.2 and 4324.0 nA (Figure 3C). When WSe_2 was loaded on AuNPs/GDY/GE, the photocurrent response enhanced to 247.8 and 9574.0 nA (Figure 3D). It is due to the enhancement effect of WSe_2 toward AuNPs/GDY. These comparison results indicated that WSe_2 and AuNPs/GDY can be employed as a preferable photoactive material for construction of the PEC biosensor. Remarkably, the background signal produced by AuNPs/GDY is low (27.6 nA), so it is beneficial to the improvement of sensitivity.

The PEC response of the signal indicator was measured (Figure 4A). The PEC signals of WSe_2 (Figure 4A, curve a) and MBA/WSe_2 (Figure 4A, curve b) were 150.2 and 141.8 nA, respectively. Then, the photocurrent response improved to 2593.0 nA when the electron donor, DA, was assembled onto MBA/WSe_2 (Figure 4A, curve c). The results indicated that the signal indicator, DA/MBA/WSe_2, was successfully synthesized. DA/MBA/WSe_2 was also authenticated by Fourier transform infrared spectroscopy (FT-IR) (Figure

https://doi.org/10.1021/acsami.1c07617
ACS Appl. Mater. Interfaces 2021, 13, 26515−26521

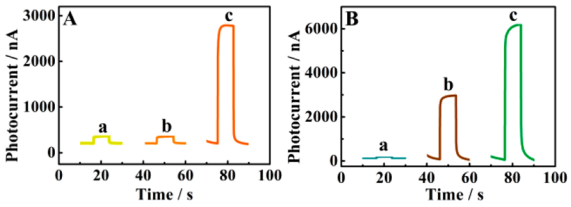

Figure 4. (A) Photocurrent characterization of the step-by-step construction of the signal indicator: WSe_2 (a), MBA/WSe_2 (b), and DA/MBA/WSe_2 (c). (B) PEC responses of the AuNPs/GDY/GE (a) and the AuNPs/GDY/GE incubated with different signal indicators: DA/Cys/WSe_2 (b) and DA/MBA/WSe_2 (c).

2C). The disappearance of the characteristic absorption peak of S−H at 2566 cm^{-1} (Figure 2C, curve b) and the peak of phenolic hydroxyl at 1280 cm^{-1} (Figure 2C, curve c) confirmed the formation MBA/WSe_2. The details are displayed in Supporting Information S8. In our previous work,[7] the signal indicator, DA/Cys/WSe_2, was obtained with an amidation reaction by using DA as the electron donor being connected to WSe_2 nanosheets via L-cysteine (Cys) (annotated as the Cys-linking strategy). In this work, the signal indicator, DA/MBA/WSe_2, is composed of WSe_2 nanoflower and DA. But as an improvement, MBA is used as an alternate connecting unit for linking DA and the WSe_2 nanoflower (called the MBA-linking strategy). In comparison with the Cys-linking strategy, the MBA-linking strategy is more attractive, benefiting from its advantages such as easy operation and shorter reaction time. More importantly, the PEC signal was enhanced. At first, AuNPs/GDY was modified onto the GE. Then, 10 μL of DA/MBA/WSe_2 or DA/Cys/WSe_2 was dropped onto the surface of the AuNPs/GDY/GE, separately. The photocurrent response of AuNPs/GDY/GE is very low (Figure 4B, curve a). When the signal indicator was loaded, the photocurrent response increased sharply. Evidently, the photocurrent response of the signal indicator made by the MBA-linking strategy is 6153.2 nA (Figure 4B, curve c), which is almost twice that made by the Cys-linking strategy (Figure 4B, curve b, 2978.3 nA). This shows that under the same conditions DA/MBA/WSe_2 can give a higher PEC signal, thus obtaining greater photocurrent response and higher sensitivity.

Photogenerated Electron−Hole Transfer Mechanism of the Biosensing System. The rapid rise of the photocurrent response of WSe_2−AuNPs/GDY under irradiation is indicative that the fast charge generation, separation, and transfer correlate with the surface chelating. In order to validate the possible charge-transfer process of this system, cyclic voltammetry (CV) was conducted to estimate the conduction band (CB) and valence band (VB) of the WSe_2 and GDY (Figure 5). The band positions versus the saturated calomel electrode (SCE) are assigned from the onset oxidation/reduction potential by using the following formulas:[31,32]

$$E_{CB/LUMO} = -(E_{red} + 4.74)\ eV \quad (1)$$

$$E_{VB/HOMO} = -(E_{ox} + 4.74)\ eV \quad (2)$$

$$E_{VB/HOMO} = E_{CB/LUMO} - E_{gap} \quad (3)$$

The band positions and band gap values (E_{gap}) calculated by the CV measurements are displayed in Table 1. The results indicated that GDY is a narrow band gap material, and the

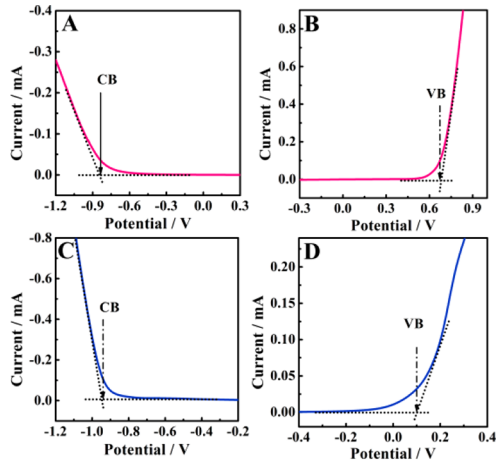

Figure 5. Cathodic and anodic linear potential scans for determining the CB and VB of the WSe_2 nanoflower (A and B) and GDY (C and D) at 0.005 V s^{-1} in 0.1 M pH 7.4 phosphate buffer.

band gap is 1.04 eV, approximately in accordance with the previously report.[8,33,34] The band gap of WSe_2 is 1.51 eV.

The mechanism of PEC signal generation is displayed in Scheme 2. Upon light excitation, the electron−hole pairs are produced from the WSe_2 nanoflower and GDY. Obviously, the CB and the VB of WSe_2 are more negative than those of GDY. This thermodynamic condition facilitates to fancily transfer photoinduced electrons that accumulate on the CB of WSe_2 into the CB of GDY. Such a synergy effect between the WSe_2 nanoflower and GDY can reduce the photoinduced electron−hole recombination and expedite the spatial charge separation. On the other hand, the incorporation of AuNPs also facilitates charge transport and enhances the excitation and conversion efficiency. Moreover, the photoinduced holes in the VB of WSe_2 participate in the oxidation reaction of DA, and prolong the lifetime of the electron−hole pairs, which is favorable to improve the PEC performance.

Characterization of the Biosensor Fabrication Process. For the investigation of the preparation process of the biosensor, impedance spectroscopy (EIS) was performed under a potential of 0.22 V and a frequency range of 10^{-2}−10^6 Hz (Figure 6A). In comparison to the bare GE (Figure 6A, curve a), the AuNPs/GD/GE (Figure 6A, curve b) presents a decreased R_{et}, because of the augmentation of the specific surface area and acceleration of electron-transfer efficiency. After the assembly of TsDNA, as expected, the R_{et} increased (Figure 6A, curve c) because of the effective electrostatic repulsion between the negatively charged DNA framework and $[Fe(CN)_6]^{3-/4-}$. The modification of nonconductive 6-mercaptohexanol (MCH) leads to the R_{et} being enhanced markedly (Figure 6A, curve d). When FT and the PEC nanoprobe were step-by-step incubated with MCH/TsDNA/AuNPs/GDY/GE, the R_{et} value increased to 526.7 Ω (Figure 6A, curve e). The interface property of the modified electrode was also step-by-step characterized by CV in 5.0 mM $[Fe(CN)_6]^{3-/4-}$. The bare GE (Figure 6B, curve a) showed a pair of reversible redox peaks. With AuNPs/GDY coated onto the electrode surface (Figure 6B, curve b), the peak current value increased obviously. After the introduction of TsDNA (Figure 6B, curve c) a decrease of the peak current was induced, owing to the poor electrical conductivity of TsDNA. The oxidation peak current further decreased because of the impediment of MCH immobilized onto the above

https://doi.org/10.1021/acsami.1c07617
ACS Appl. Mater. Interfaces 2021, 13, 26515−26521

Table 1

material	E_{red} vs SCE (V)[a]	E_{ox} vs SCE (V)	$E_{CB/LUMO}$ (eV)	$E_{VB/HOMO}$ (eV)	E_{gap} (eV)
WSe_2	−0.82	0.69	−3.92	−5.43	1.51
GDY	−0.94	0.10	−3.80	−4.84	1.04

[a]SCE: saturated calomel electrode.

Scheme 2. Photocurrent Generation Mechanism

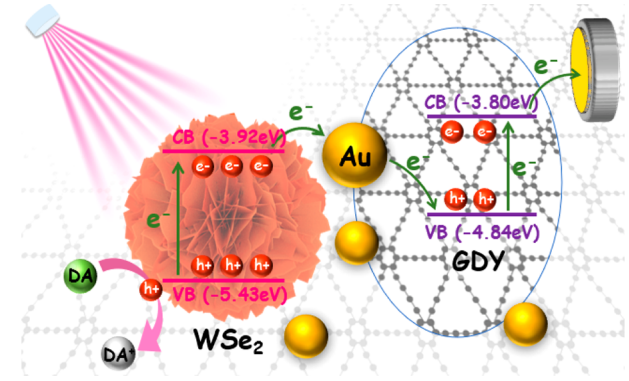

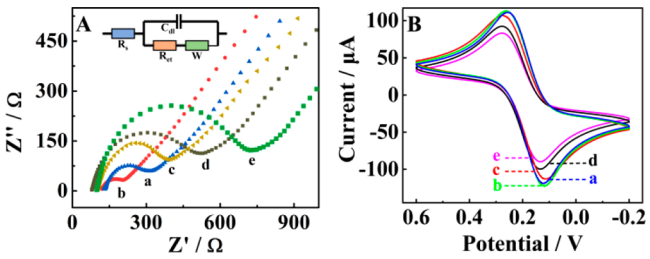

Figure 6. (A) EIS and (B) CV of different electrodes: bare GE (a), AuNPs/GDY/GE (b), TsDNA/AuNPs/GDY/GE (c), and MCH/TsDNA/AuNPs/GDY/GE (d), after MCH/TsDNA/AuNPs/GDY/GE was incubated with FT and the PEC nanoprobe (e).

electrode (Figure 6B, curve d). After incubation with FT and the PEC nanoprobe, the oxidation peak current diminishes ulteriorly (Figure 6B, curve e). The obtained results indicate the successful construction of the biosensor.

PEC Response for the α-Synuclein Oligomer. Under the optimal experiment conditions (Figures S5 and S6), the analytical characteristics of the PEC biosensor were investigated by quantitatively detecting various concentrations of α-Syn oligomer. As depicted in Figure 7A, the PEC response linearly increased as the logarithm of α-Syn oligomer concentration increased from 10 aM to 1.0 nM with a

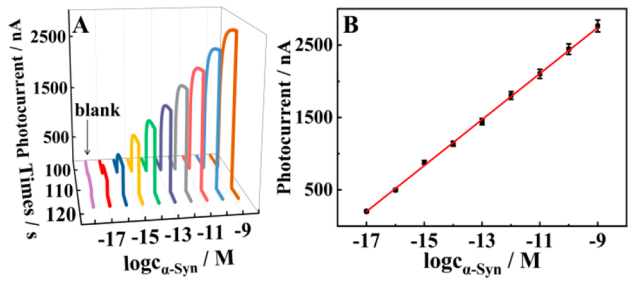

Figure 7. PEC responses of the biosensor corresponding to various concentrations of α-Syn oligomer (A) and the corresponding calibration plot between the PEC response and logarithm of α-Syn oligomer concentration (B).

detection limit of 3.3 aM [defined as LOD = 3(S/N)]. The linear regression equation was fitted to I = 1020.8 log c + 17365.3, with a correlation coefficient of 0.9959 [I and c represent the PEC response (nA) and the concentration of α-Syn oligomer (M), respectively] (Figure 7B). The relative standard deviation (RSD) is 3.7% at 100 aM. A comparison between this method with previous reports was explored. As shown in Table S2, this method had a wide detection range and a low detection limit.

Specificity is a key index for the assessment of biosensor performance. Several potential interferences, such as glucose dehydrogenase (PQQGDH), C-reactive protein (CRP), luciferase, and immunoglobulin G (IgG), are used to assess the specificity. The concentrations of interferences are 100 times larger than the α-Syn oligomer concentration. A low PEC response, nearly that of a blank test, is observed when PQQGDH, CRP, luciferase, and IgG are used as the detection sample (Figure 8A). As expected, a significant PEC response

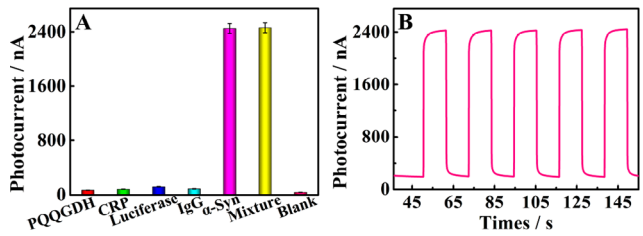

Figure 8. (A) Specificity of the PEC biosensor toward different interferences (n = 7). (B) Stability monitoring of the PEC biosensor.

was achieved for α-Syn oligomer and the mixture containing α-Syn oligomer, PQQGDH, CRP, luciferase, and IgG. These results revealed the specificity of the PEC biosensor to detect α-Syn oligomer and showed that the signal generated was owing to the specific binding of α-Syn oligomer to the aptamer.

Furthermore, the PEC biosensor incubated with 100 pM α-Syn oligomer was implemented under continuous scanning for five cycles to investigate the stability (Figure 8B). The PEC response revealed an inconspicuous change during the cycles, and the RSD was 2.4%, which demonstrated that this PEC biosensor has excellent stability.

Practical Sample Detection. The applicability and feasibility of the biosensor for α-Syn oligomer detection were confirmed by the sample standard addition method. In order to avoid the interference of the background signal, different amounts of α-Syn oligomer were added to the human serum after 100 times of dilution. Then, a recovery experiment was carried out, and the standard addition method was used to detect α-Syn oligomer doped at different concentrations. The results in Table S3 clearly indicate that the recovery rate is between 98.9% and 110.0%, and the RSD's are between 2.36% and 4.02%, demonstrating that this biosensor has potential ability for auxiliary clinical diagnosis.

https://doi.org/10.1021/acsami.1c07617
ACS Appl. Mater. Interfaces 2021, 13, 26515−26521

CONCLUSIONS

A PEC biosensor based on a AuNPs/GDY-modified electrode and DA/MBA/WSe_2 as the signal indicator was successfully fabricated. α-Synuclein oligomer was detected sensitively by coupling with a dual-cycle amplification strategy. In this PEC biosensor, target triggered cycle I and achieved the conversion of α-Syn oligomer to a massive output of FT. The output FT was used for cycle II onto the AuNPs/GDY and TsDNA modified electrode. The ultralow blank and high PEC signal were achieved due to the intrinsic PEC property of GDY and the specific device of the signal indicator for the PEC signal enhancement. As expected, this PEC biosensor was applied to the detection of α-Syn oligomer with good results. This strategy both provided a sophisticated PEC signal indicator and exhibited an encouraging ideal for PEC biosensor delineation.

ASSOCIATED CONTENT

Supporting Information

The Supporting Information is available free of charge at https://pubs.acs.org/doi/10.1021/acsami.1c07617.

Experimental section, reagents, and apparatus, synthesis and exfoliation of GDY, fabrication of the modified electrode, PEC measurement, PEC response of the photoactive materials, nucleic acids sequence, method comparison, sample test, SEM, TEM, and FT-IR, experimental conditions, and principle of cycle II (PDF)

AUTHOR INFORMATION

Corresponding Author

Xu Hun − *Key Laboratory of Sensor Analysis of Tumor Marker, Ministry of Education, College of Chemistry and Molecular Engineering, Qingdao University of Science and Technology, Qingdao 266042, People's Republic of China;* orcid.org/0000-0001-5793-067X; Email: hunxuprof@outlook.com; Fax: +86-532-84022681

Authors

Ting Yao − *Key Laboratory of Sensor Analysis of Tumor Marker, Ministry of Education, College of Chemistry and Molecular Engineering, Qingdao University of Science and Technology, Qingdao 266042, People's Republic of China*

Ruhao Wang − *Key Laboratory of Sensor Analysis of Tumor Marker, Ministry of Education, College of Chemistry and Molecular Engineering, Qingdao University of Science and Technology, Qingdao 266042, People's Republic of China*

Yuchan Meng − *Key Laboratory of Sensor Analysis of Tumor Marker, Ministry of Education, College of Chemistry and Molecular Engineering, Qingdao University of Science and Technology, Qingdao 266042, People's Republic of China*

Complete contact information is available at: https://pubs.acs.org/10.1021/acsami.1c07617

Notes

The authors declare no competing financial interest.

ACKNOWLEDGMENTS

The authors gratefully acknowledge the support of NSFC (21575073) and the Laoshan Scholar Program of Qingdao University of Science and Technology (201802685).

REFERENCES

(1) Chikkaveeraiah, B. V.; Bhirde, A. A.; Morgan, N. Y.; Eden, H. S.; Chen, X. Electrochemical Immunosensors for Detection of Cancer Protein Biomarkers. *ACS Nano* **2012**, *6* (8), 6546−6561.

(2) Xi, X.; Li, T.; Huang, Y.; Sun, J.; Zhu, Y.; Yang, Y.; Lu, Z. J. Rna Biomarkers: Frontier of Precision Medicine for Cancer. *Non-coding RNA* **2017**, *3* (1), 9.

(3) Bell, J. Predicting Disease Using Genomics. *Nature* **2004**, *429* (6990), 453−456.

(4) Hao, Q.; Shan, X.; Lei, J.; Zang, Y.; Yang, Q.; Ju, H. A Wavelength-Resolved Ratiometric Photoelectrochemical Technique: Design and Sensing Applications. *Chem. Sci.* **2016**, *7* (1), 774−780.

(5) Zhao, W.-W.; Xu, J.-J.; Chen, H.-Y. Photoelectrochemical Immunoassays. *Anal. Chem.* **2018**, *90* (1), 615−627.

(6) Yu, X.; Prévot, M. S.; Guijarro, N.; Sivula, K. Self-Assembled 2d Wse2 Thin Films for Photoelectrochemical Hydrogen Production. *Nat. Commun.* **2015**, *6* (1), 7596.

(7) Yao, T.; Hun, X. A Design for the Photoelectrochemical Detection of Mirna-221 Based on a Tungsten Diselenide−Cysteine−Dopamine Nanoprobe Coupled with Mismatched Catalytic Hairpin Assembly Target Recycling with Ultra-Low Background Noise. *Chem. Commun.* **2019**, *55* (70), 10380−10383.

(8) Zhang, Y.; Xiao, J.; Xie, X.; Chen, H.; Deng, S. Layer Dependence of the Photoelectrochemical Performance of a Wse2 Photocathode Characterized Using in Situ Microscale Measurements. *RSC Adv.* **2019**, *9* (53), 30925−30931.

(9) Lewis, N. S. Developing a Scalable Artificial Photosynthesis Technology through Nanomaterials by Design. *Nat. Nanotechnol.* **2016**, *11* (12), 1010−1019.

(10) Li, J.; Gao, X.; Liu, B.; Feng, Q.; Li, X.-B.; Huang, M.-Y.; Liu, Z.; Zhang, J.; Tung, C.-H.; Wu, L.-Z. Graphdiyne: A Metal-Free Material as Hole Transfer Layer to Fabricate Quantum Dot-Sensitized Photocathodes for Hydrogen Production. *J. Am. Chem. Soc.* **2016**, *138* (12), 3954−3957.

(11) Wang, S.; Yi, L.; Halpert, J. E.; Lai, X.; Liu, Y.; Cao, H.; Yu, R.; Wang, D.; Li, Y. A Novel and Highly Efficient Photocatalyst Based on P25−Graphdiyne Nanocomposite. *Small* **2012**, *8* (2), 265−271.

(12) Li, J.; Wang, C.; Zhang, B.; Wang, Z.; Yu, W.; Chen, Y.; Liu, X.; Guo, Z.; Zhang, H. Artificial Carbon Graphdiyne: Status and Challenges in Nonlinear Photonic and Optoelectronic Applications. *ACS Appl. Mater. Interfaces* **2020**, *12* (44), 49281−49296.

(13) Nulakani, N. V. R.; Subramanian, V. Cp-Graphyne: A Low-Energy Graphyne Polymorph with Double Distorted Dirac Points. *ACS Omega* **2017**, *2* (10), 6822−6830.

(14) Pieri, L.; Madiona, K.; Melki, R. Structural and Functional Properties of Prefibrillar A-Synuclein Oligomers. *Sci. Rep.* **2016**, *6* (1), 24526.

(15) El-Agnaf, O. M. A.; Salem, S. A.; Paleologou, K. E.; Curran, M. D.; Gibson, M. J.; Court, J. A.; Schlossmacher, M. G.; Allsop, D. Detection of Oligomeric Forms of A-Synuclein Protein in Human Plasma as a Potential Biomarker for Parkinson's Disease. *FASEB J.* **2006**, *20* (3), 419−425.

(16) Tsukakoshi, K.; Abe, K.; Sode, K.; Ikebukuro, K. Selection of DNA Aptamers That Recognize A-Synuclein Oligomers Using a Competitive Screening Method. *Anal. Chem.* **2012**, *84* (13), 5542−5547.

(17) van Rumund, A.; Green, A. J. E.; Fairfoul, G.; Esselink, R. A. J.; Bloem, B. R.; Verbeek, M. M. A-Synuclein Real-Time Quaking-Induced Conversion in the Cerebrospinal Fluid of Uncertain Cases of Parkinsonism. *Ann. Neurol.* **2019**, *85* (5), 777−781.

(18) Leung, C. W. T.; Guo, F.; Hong, Y.; Zhao, E.; Kwok, R. T. K.; Leung, N. L. C.; Chen, S.; Vaikath, N. N.; El-Agnaf, O. M.; Tang, Y.; Gai, W.-P.; Tang, B. Z. Detection of Oligomers and Fibrils of A-Synuclein by Aiegen with Strong Fluorescence. *Chem. Commun.* **2015**, *51* (10), 1866−1869.

(19) Li, C.; Lutz, E. A.; Slade, K. M.; Ruf, R. A. S.; Wang, G.-F.; Pielak, G. J. 19f Nmr Studies of A-Synuclein Conformation and Fibrillation. *Biochemistry* **2009**, *48* (36), 8578−8584.

(20) Sun, K.; Xia, N.; Zhao, L.; Liu, K.; Hou, W.; Liu, L. Aptasensors for the Selective Detection of Alpha-Synuclein Oligomer by Colorimetry, Surface Plasmon Resonance and Electrochemical Impedance Spectroscopy. *Sens. Actuators, B* **2017**, *245*, 87−94.
(21) Khatri, A.; Punjabi, N.; Ghosh, D.; Maji, S.; Mukherji, S. Detection of A-Synuclein, Marker for Parkinson's Disease Using Localized Surface Plasmon Resonance Fiber Optic Sensor. In *International Conference on Fibre Optics and Photonics 2014*, Proceedings of the 12th International Conference on Fiber Optics and Photonics, Kharagpur, India, 2014/12/13; OSA Publishing: Washington, DC, 2014; p M4A.45.
(22) Guo, S.; Jiang, Y.; Wu, F.; Yu, P.; Liu, H.; Li, Y.; Mao, L. Graphdiyne-Promoted Highly Efficient Photocatalytic Activity of Graphdiyne/Silver Phosphate Pickering Emulsion under Visible-Light Irradiation. *ACS Appl. Mater. Interfaces* **2019**, *11* (3), 2684−2691.
(23) Li, G.; Li, Y.; Liu, H.; Guo, Y.; Li, Y.; Zhu, D. Architecture of Graphdiyne Nanoscale Films. *Chem. Commun.* **2010**, *46* (19), 3256−3258.
(24) Gan, W.; Xu, B.; Dai, H.-L. Super Bright Luminescent Metallic Nanoparticles. *J. Phys. Chem. Lett.* **2018**, *9* (15), 4155−4159.
(25) Liu, S.; Du, Z.; Li, P.; Li, F. Sensitive Colorimetric Visualization of Dihydronicotinamide Adenine Dinucleotide Based on Anti-Aggregation of Gold Nanoparticles Via Boronic Acid−Diol Binding. *Biosens. Bioelectron.* **2012**, *35* (1), 443−446.
(26) Zhang, L.; Cheng, Y.; Lei, J.; Liu, Y.; Hao, Q.; Ju, H. Stepwise Chemical Reaction Strategy for Highly Sensitive Electrochemiluminescent Detection of Dopamine. *Anal. Chem.* **2013**, *85* (16), 8001−8007.
(27) Tomsho, J. W.; Benkovic, S. J. Elucidation of the Mechanism of the Reaction between Phenylboronic Acid and a Model Diol. *J. Org. Chem.* **2012**, *77* (5), 2098−2106.
(28) Hun, X.; Liu, B.; Meng, Y. Ultrasensitive Chemiluminescence Assay for the Lung Cancer Biomarker Cytokeratin 21−1 Via a Dual Amplification Scheme Based on the Use of Encoded Gold Nanoparticles and a Toehold-Mediated Strand Displacement Reaction. *Microchim. Acta* **2017**, *184* (10), 3953−3959.
(29) Liu, Z.; Zhao, H.; Li, N.; Zhang, Y.; Zhang, X.; Du, Y. Assembled 3d Electrocatalysts for Efficient Hydrogen Evolution: Wse2 Layers Anchored on Graphene Sheets. *Inorg. Chem. Front.* **2016**, *3* (2), 313−319.
(30) Wang, X.; Chen, Y.; Zheng, B.; Qi, F.; He, J.; Li, Q.; Li, P.; Zhang, W. Graphene-Like Wse2 Nanosheets for Efficient and Stable Hydrogen Evolution. *J. Alloys Compd.* **2017**, *691*, 698−704.
(31) Barman, M. K.; Mitra, P.; Bera, R.; Das, S.; Pramanik, A.; Parta, A. An Efficient Charge Separation and Photocurrent Generation in the Carbon Dot−Zinc Oxide Nanoparticle Composite. *Nanoscale* **2017**, *9* (20), 6791−6799.
(32) Bera, R.; Jana, B.; Mondal, B.; Patra, A. Design of Cdtese−Porphyrin−Graphene Composite for Photoinduced Electron Transfer and Photocurrent Generation. *ACS Sustainable Chem. Eng.* **2017**, *5* (4), 3002−3010.
(33) Li, X.; Li, Y.; Zhang, J.; Meng, Y.; Yu, X.; Wang, X.; Hun, X. Molybdenum Disulfide/Graphdiyne-Based Photoactive Material Derived Photoelectrochemical Strategy for Highly Sensitive Microrna Assay. *Sens. Actuators, B* **2019**, *297*, 126808.
(34) Bu, H.; Zhao, M.; Zhang, H.; Wang, X.; Xi, Y.; Wang, Z. Isoelectronic Doping of Graphdiyne with Boron and Nitrogen: Stable Configurations and Band Gap Modification. *J. Phys. Chem. A* **2012**, *116* (15), 3934−3939.

https://doi.org/10.1021/acsami.1c07617
ACS Appl. Mater. Interfaces 2021, 13, 26515−26521